Fuel 372 (2024) 132146

Contents lists available at ScienceDirect

Fuel

journal homepage: www.elsevier.com/locate/fuel

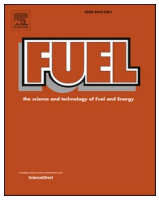

Full Length Article

CO_2-rich and CO_2-lean streams as activators of reducing metals for the green hydrogen generation and the catalytic production of formate

Juan I. del Río [a,b], Miguel Almarza [a], Ángel Martín [a,*], María D. Bermejo [a]

[a] BioEcoUva, Bioeconomy Research Institute, PressTech Group, Department of Chemical Engineering and Environmental Technology, Universidad de Valladolid, Prado de la Magdalena s/n, 47011 Valladolid, Spain
[b] Grupo Procesos Químicos Industriales, Department of Chemical Engineering, Universidad de Antioquia UdeA, Calle 70 No. 52-21, Medellín 050010, Colombia

ARTICLE INFO

Keywords:
Catalysts assessment
CO_2 utilization
Hydrogen evolution
Formic acid production
Metal-water splitting

ABSTRACT

The ongoing pursuit of carbon mitigation and utilization encourages the study of common and more abundant materials, capable of facilitating the technical readiness of the processes involved. In this context, the present work aims at evaluating the CO_2-rich and CO_2-lean streams from the basic aqueous absorption CO_2 capture processes, for the *in-situ* generation of green hydrogen through the metal-water splitting technology, to convert captured CO_2 into formate. Experiments have been carried out using aluminum and zinc as reducing agents, and the commercial catalysts palladium, platinum and ruthenium supported on activated carbon, using a batch stirred reactor. Aluminum and Pd5AC constituted the best metal/catalyst system, with a formate yield of 22 %, selectivity of 32 %, and conversion of 67 %. The H_2-TPR characterization of the catalysts, before and after reaction, showed that only Pd5AC catalyst shows insights of active hydride specie, responsible for the reduction of captured CO_2. The *in-situ* hydrogen evolution was studied during prolonged 10 h experiments, in absence of catalyst, to compare the performance of the proposed basic streams and reducing metals, generating high reliability data in search for feasibility and future integration of CO_2 and H_2 economies.

1. Introduction

Current changes in worldwide economic scenario are challenging the achievement of the past-decades objectives of cutting the CO_2 emissions and reducing oil and natural gas dependency. The increase of demand of fossil fuels in 2040 can increase up to 30 % [1], and the necessity of mitigating the subsequent CO_2 emissions is still on the table. In this context, one of the most successful carbon capture and storage (CCS) technologies is the absorption of CO_2 with aqueous solutions of ammonia (generally any basic dissolution used for CO_2 capture is known as CO_2 Capture-Solvent Lean stream, CO2LS, in absorber/stripper columns, yielding a CO_2-Rich stream, CO2RS) containing an equilibria of ammonia bicarbonate, carbonate and carbamate [2,3]. Once captured, CO_2 can be stored for example in depleted oil and gas fields, or in deep saline aquifer formations and in deep coal seams that cannot be mined anymore and are widely distributed around the world in sedimentary basins, usually several kilometers below the earth's surface [3]. To store CO_2, it must be transported from the production site to the place of storage or use. CO_2 is transported via gas pipelines, ships or trains, depending on how economical the means of transport are [4].

In addition to capturing and storing CO_2, there are different CO_2 utilization approaches, framed in the so-called *CO_2-Economy*. In the first place, CO_2 can be used directly without no chemical conversion in applications such as refrigerant (supercritical state), in food and beverages, as fire extinguisher, in concrete materials, in oil wells, pharmaceuticals, as a solvent or antisolvent, etc [5]. In the second place, its indirect utilization implies the chemical transformation into other compounds, such as useful chemicals and fuels [6–8]. CO_2-derived fuels with high energy density are gaining more attention as energy vectors for fulfilling the energy storage demands [9], where formic acid (FA), methane and methanol are prominent [10–12].

Hydrothermal catalytic reduction of captured CO_2 using reducing metals is one of the methods to obtain formic acid that remains on the research focus [13,14]. The method starts with the *in-situ* generation of H_2, by metal-water splitting, with the subsequent reduction of CO_2 in presence of catalyst, following the overall reaction pathway [13]:

$$M^0 + H_2O \rightarrow M_xO_y + H_2 + CO_2 \rightarrow HCOOH \quad (1)$$

where M^0 is a reducing metal (e.g. aluminum and zinc). In our most

* Corresponding author.
E-mail address: angel.martin.martinez@uva.es (Á. Martín).

https://doi.org/10.1016/j.fuel.2024.132146
Received 20 March 2024; Received in revised form 31 May 2024; Accepted 5 June 2024
Available online 14 June 2024

recent work, the endeavors laid the implementation of milder reactions conditions for ammonia-based CO_2 absorption derivatives, while contrasting its performance toward more common substrates like sodium bicarbonate, using commercial Pd 5 wt% over activated carbon catalyst [15]. Likewise, catalytic metals like ruthenium displayed high efficiency in reducing CO_2 to formate when supported on alumina or activated carbon, using sodium bicarbonate as a source of CO_2, at 80 °C, 5 MPa of H_2 and a reaction time of one hour [16]. This study concluded that the optimum ruthenium content is 2 % because higher ruthenium percentages reduce its Turnover Number (TON). González *et al.* [17] compared the performance of activated carbon-supported catalysts, loaded with 5 wt% of metals Pd, Ru, Ni, Co and Re, on the reduction of sodium bicarbonate to formate in a semi-continuous flow reactor, at 25 °C and 0.1 MPa of hydrogen. The catalytic activity decreased in the order Pd/C > Ru/C > Ni/C > Re/C ≈ Co/C, reaching a marginal formate molar yield (carbon-based) up to ~3.7 % after 72 h, with Pd/C. Not many antecedents are available for Pt based catalyst in the reduction of captured CO_2 with reducing metals, though abundant reports are available for electrochemical and photocatalytical conversion of CO_2 [18–21]. However, the reduction of captured CO_2 by Pt based catalyst into formate has been proved with glycerol as reducing agent [22]. Based on the review by Gunasekar *et al.* [23], compared to other possible catalytic supports, such as $BaSO_4$, $CaCO_3$ and γ-Al_2O_3, the activated carbon exhibited better catalytic performance, thanks to its hydrophobic nature that allows accumulation of H_2 on the support's surface.

Other advances have been recently accomplished with homogeneous catalysts containing Ru, Rh or Ir [24,25], displaying high selectivity and yield to formate, even at mild conditions, but still dealing with several drawbacks when facing industrial scale up, concerning the separation and recyclability of these catalysts [26].

On the other hand, metals used as reductants for CO_2 hydrogenation are of great interest to be utilized as *in-situ* reducing agents, generating molecular hydrogen by the metal water-splitting reaction, that is favored under alkaline conditions [27]. In this matter, aluminum and zinc are beneficial to this process because they are two of the most abundant metals, with high availability in the market, and can be also found as residues at a low cost. The byproducts generated from water-splitting reaction are hydroxides and metal oxides, which for the case of Al and Zn are of great interest in catalysis industry and water treatment. For aluminum, the main subproduct is aluminum hydroxide (boehmite), which is a precursor for production of alumina [28], a well-known material as support in catalysis; and zinc hydroxide is used as a precursor for the preparation of zinc hydroxy stannate materials as catalyst for photodegradation of harmful organic dye [29]. Al and Zn hydroxides/oxides provide excellent adsorption capacities of phosphate from wastewater, due to their excellent adsorption capacities, good reaction kinetics and selectivity [30]. However, on the light of a circular-economy and zero-emissions practice, in the field of CO_2 hydrogenation it would make more sense to reduce these oxidated byproducts back to the zero-valent metals for reutilization, in a process driven by solar power [31]. In this process, the hydrogen produced from water can be categorized as green, if using renewable energy sources in the process without carbon emissions [32].

It is clear that the reduction of captured CO_2 as bicarbonate using reducing metals like Mn, Al and Zn, have shown effectiveness, displaying yields up to 81 % and 2 h [10,33]. Despite these works, not much literature is available about the comparison of different supported metal catalysts, reducing metals and CO2RS/CO2LS streams on the simultaneous reduction of captured CO_2 from the ammonia-based process and hydrogen generation from metal-water splitting reaction.

The present study aims at two main objectives: i) studying the generation of hydrogen with different metal/catalyst systems and CO2RS/CO2LS, by means of a hydrogen evolution analysis during prolonged experiments (10 h), in absence of catalyst, and ii) ii) evaluating different commercial catalysts in the reduction of captured CO_2 by an energy-efficient technology like the aqueous ammonia absorption, where the hydrogen needed is generated by a metal-water splitting reaction *in-situ*, forming the metal/catalyst system. These studies are important because they allow screening different catalysts for the reduction process, while understanding the influence of the reaction media on the hydrogen generation. Also, they allow determining the most active catalyst and metals for CO_2 reduction and H_2 generation *in situ*, a broadened study compared to previous publications using only one catalyst and reducing metal [15]. These results will feed potential integrations of carbon capture processes and the green hydrogen production in the frame CO_2 and hydrogen economies.

2. Materials and methods

2.1. Chemicals

As CO_2-Rich streams (CO2RS), ammonium carbamate (AC) (99 %) and sodium bicarbonate (SB) (100 %) diluted in water MilliQ were used at 0.5 mol/L. As CO_2-Lean stream (CO2LS), an aqueous solution of ammonia at 0.5 mol/L was used. Fine powders of commercial Pd/C catalyst of 5 wt% (Pd5AC), Pt/C catalyst of 5 wt% (Pt5AC) and Ru/C catalyst of 5 wt% (Ru5AC) were used as received. The reducing metals used were aluminum powder (Al) (99.5 %) and zinc powder (Zn) (99.5 %). Activated charcoal RX3-Extra (Norit) was used for catalyst support blank experiments. All reagents, except aluminum powder (Goodfellow), sodium bicarbonate (COFARCAS-Spain), and ammonia (Panreac) were purchased from Sigma-Aldrich. Hydrogen (99.99 %) was provided by Linde.

2.2. Experiments for hydrogen generation

In order to evaluate the effect of both CO2RS and CO2LS on the hydrogen generation, batch experiments were conducted in absence of catalyst for 10 h at 120 °C, using 24 mmol of Al or Zn, in 0.5 mol/L aqueous solution of carbamate (initial pH = 9.2), sodium bicarbonate (initial pH = 10.1) (as CO2RS), or NH_3 (initial pH = 11.5) (as CO2LS), using a Parr Instruments stainless steel reactor (25 mL Micro Stirred Reactors Series 4791, maximum pressure 20 MPa, maximum temperature 350 °C) with stirring at 700 rpm, autogenous pressure, and ramp heating of 14 °C/min, equipped with a band heater. Gas samples were taken in intervals of 2 h, using Tedlar® bags, to quantify the hydrogen concentration by GC-TCD. In these experiments, a reduced liquid filling volume percentage of 25 % was employed to avoid draining out of liquid and solids when sampling the gas, due to the depressurization.

2.3. Experiments for catalysts assessment

The comparison of the different metals as hydrogen source from water, as well as the evaluation of the selected catalysts for the conversion of capture CO_2 were carried out in batch, using the same Parr reactor. Before each run, metals and catalysts were weighed, and physically mixed inside the batch reactor. Ammonium carbamate was weighed and diluted in water so that its initial concentration was 0.5 mol/L. Once the reactor was sealed, a gentle flow of nitrogen was passed through the headspace to purge the remaining air out of the system, followed by heating up, at 14 °C/min, to a constant temperature of 120 °C. Once reached, reaction proceeded for 2 h. After the reaction, the vessel was quickly immersed in a water bath to cool it down to room temperature, followed by collection of liquid and gas samples for formate and hydrogen quantification. For the catalytic experiments, conditions were fixed to 6 mol of reducing metal per carbamate mole, 3.8 mmol of catalyst metal (for a comparison basis of metals Pd, Ru, Pt) per mole of carbamate, and 70 % of the volume of the reactor filling at room temperature. Experiments with pure-hydrogen (2.5 MPa of 99.99 % pure-hydrogen), instead of reducing metals (Al or Zn), were done under the same reaction conditions, to conduct reducibility analyses of the catalysts by H_2-TPR technique. Experiments were duplicated to

establish experimental uncertainty.

2.4. Products characterization

2.4.1. Liquids

Once the reactor was cooled down, the liquid sample was collected and filtered through a 0.22 mm filter. For quantification of formic acid (FA), carbamate and sodium bicarbonate concentrations, the liquid samples were analyzed by HPLC (Waters, Alliance separation module e2695) using an RAZEX™ ROA-Organic Acid H + column with RI detector (Waters, 2414 module). The mobile phase was 25 mM H_2SO_4 with a flow rate of 0.5 mL/min. The temperatures of the column and the detector were 40 °C and 30 °C, respectively.

The yield and selectivity of formic acid, as well as conversion of the carbamate were calculated as in Eqs. (2) to (4). Turnover number (TON) is a useful parameter to evaluate and compare the performance of catalysts, defined as the number of substrate moles converted to target product by mol of surface active-metal in catalyst [34], and was calculated by Eq. (5):

$$Y_{FA} = \frac{C_{FA,f}}{C_{cs,i}} x100 \tag{2}$$

$$X_{CS} = \frac{C_{cs,f} - C_{cs,i}}{Ccs,i} x100 \tag{3}$$

$$S_{FA} = \frac{Y_{FA}}{X_{CS}} x100 \tag{4}$$

$$TON = \frac{C_{cs,i} * Y_{FA}}{ncatalyst_{metal} * D} x100 \tag{5}$$

where Y_{FA} is the yield of formic acid, X_{CS} is the conversion of carbamate, S_{FA} is the selectivity of formic acid, $C_{FA,f}$ is the final molar concentration of formic acid, $C_{CS,i}$ is the initial molar concentration of carbon source, $C_{CS,f}$ is the final molar concentration of carbon source, $ncatalyst_{metal}$ is the number of moles of active metal in catalyst per liter of reaction solution, and D is the metallic dispersion, determined as described below in the solids characterization section.

2.4.2. Solids

Particle size of reducing metals, before reaction, was measured with a Malvern Mastersizer 200 laser diffraction instrument, operated in dry mode using a Scirocco accessory. Transmission electron microscopy (TEM) was performed to determine particle size and distribution of nanoparticles in raw catalysts tested, by analyzing different TEM micrographs. For that, samples were suspended on a copper grid, and analyzed in a JEOL JEM-1011 HR equipment (JEOL, Tokyo, Japan) at 100 kV.

The catalysts were also analyzed by hydrogen Temperature-Programmed Reduction (H_2-TPR), consisting of heating the samples up to 1000 °C under a flow of H_2/Ar (10 % v/v; 50 cm^3/min) at a rate of 10 °C/min, in a Autochem II 2920 Micromeritcs equipment. Hydrogen consumption was monitored by the thermal conductivity detector. Before the detector, an ice trap was used to retain any water formed during the reduction.

Metallic dispersion [35], for each active metal (Pd, Pt and Ru), was calculated by the relationship between particle size (dVA), the area per metal atom on the surface (am), the metal atomic volume (Vm) and the atomic radio (r) (Eqs. (6)–(8)):

$$D = 6\frac{Vm}{am * dVA} x100 \tag{6}$$

$$am = \pi r^2 \tag{7}$$

$$Vm = \frac{4\pi}{3} r^2 \tag{8}$$

The mean particle size (dVA) of the active metals in catalysts was determined using ImageJ 1.52a software, by measuring the length of 450–500 particles in 8–10 different TEM images, in a scale ranging between 20–1000 nm.

The solid byproducts of the reactions comprise the mixture of exhausted metal and catalyst, which could not be separated. They were characterized by X-ray diffraction (XRD). Before analysis, the samples were dried in an oven under vacuum overnight at 45 °C, to remove the remaining moisture. A BRUKER D8 DISCOVER A25 equipment was used, with 3 kW Generator, 2.2 kW type FFF Cu-ceramic tube, LynxEye Detector, operating at 40 kV and 30 mA. The database used for identifying the phases was the PDF-2 Released in 2013 (ICDD).

Textural properties analysis of the solids before reaction were conducted in an ASAP 2420 equipment with nitrogen adsorption at 77 K. All samples were degassed prior to each analysis. The surface area was determined by the BET method, and the pore size and volume by BJH method.

SEM micrographs observations were conducted over the solid byproduct after CO_2 reduction experiments, comprising a mixture of exhausted metal and catalyst, to determine the morphology and surface particle changes. For this, a Quanta 200FEG ESEM (Environmental Scanning Electron Microscope) equipment was used, operating at 20 kV. Samples were coated with gold in a K575 sputter coater, and images were generated with a BSED detector.

2.4.3. Gases

The evolution of pressure in the reaction vessel was registered by a Picotech instrument-Technology ADC-20 & TERM, attached to a pressure transducer Desin TPR-20 (error ± 0.2 MPa). Given the low pressure (<2.15 MPa) of the reaction system, its behavior can be approximated to the ideal gas, and the use of ideal gases equation is adequate. With this information, the number of mol of hydrogen produced (nH2) was calculated using Eqs. (9) and (10):

$$n\mathrm{H2} = \frac{P_{s,f} * V_{s,f}}{R * T_{s,f}} * xH2 \tag{9}$$

$$V_{s,f} = V_{s,t} - V_{s,l} \tag{10}$$

where, $P_{s,f}$ is the final absolute pressure; $T_{s,f}$ is room temperature; $V_{s,f}$ is the final overhead volume; $V_{s,t}$ is the total volume of the reaction system; $V_{s,l}$ is the final volume of liquid collected; R is the ideal gas constant (83.14472 L*mbar*K^{-1}*mol^{-1}); $xH2$ is the fractional molar composition of hydrogen, measured by a GC-TCD Varian 4900 equipment, using Molsieve 5A-10 m and Poraplot Q-10 m columns. Then, the molar yield of hydrogen (YH2) is calculated as shown in Eq. (11).

$$Y\mathrm{H2} = \frac{n\mathrm{H2}}{n\mathrm{M}} * 100 \tag{11}$$

where, nH2 is the number of mol of hydrogen produced and nM is the number of mol of reducing metal used.

3. Results and discussion

3.1. Hydrogen evolution analysis of Al and Zn under CO2RS and CO2LS

To understand the process' overall reaction (reaction 1) that lead to producing formate under the aqueous streams, it is necessary first to study the performance of metals Al and Zn in terms of H_2 evolution. To do it, batch experiments were conducted during 10 h under CO_2-Rich stream (CO2RS) (aqueous AC and SB, 0.5 mol/L), and CO_2 Capture-Solvent Lean stream (CO2LS) (aqueous NH_3, 0.5 mol/L), in absence of catalyst. Fig. 1S depicts the pressure evolution in the reactor, where the peaks observed correspond to the depressurization caused by gas samplings every 2 h. In general, Al presented faster H_2 generation rates than Zn (Fig. 1), in consonance to the formate yield results as discussed

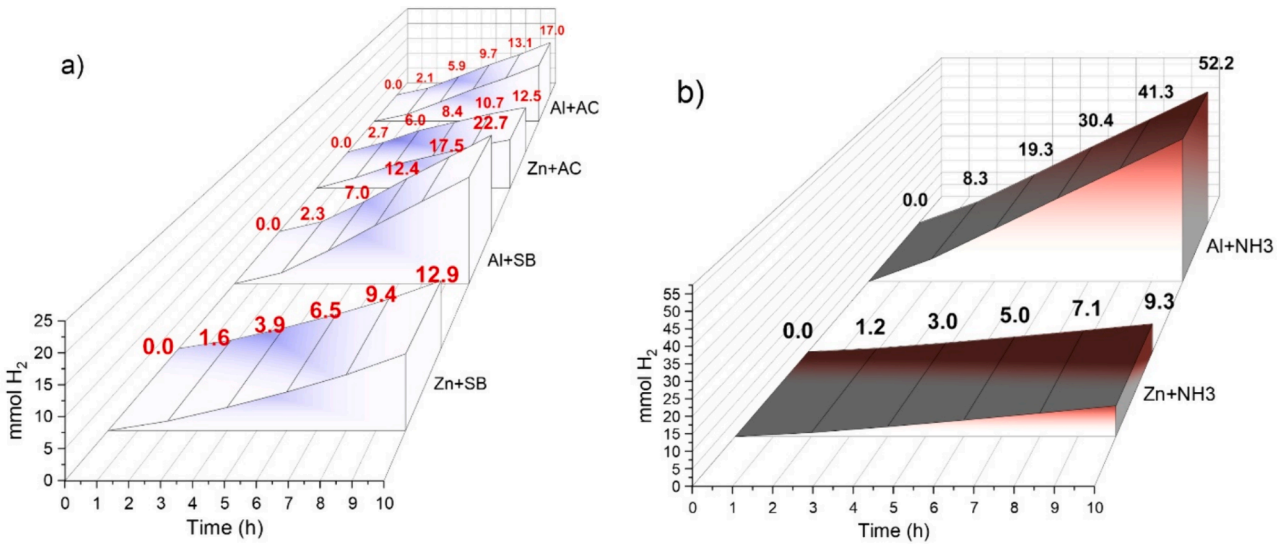

Fig. 1. H_2 evolution using Al and Zn during 10 h experiments at 120 °C, in absence of catalyst, under selected a) CO2RS (aqueous AC and SB) and b) CO2LS (aqueous NH_3).

before. A maximum of 52.2 mmol of H_2 was yielded with NH_3 in 10 h, followed by 22.7 mmol of H_2 with solvent SB and 17 mmol of H_2 with AC. Solvents NH_3 and SB have initial pH of 11.5 and 10.1, respectively, whereas for AC initial pH is 9.2, thus indicating that pH influences the hydrogen generation. From our previous work [15], a better result for SB was also observed compared to AC in the production of FA at a higher temperature of 250 °C, thus indicating that Pd5AC and aluminum powder conformed a good catalytic system for the reduction of SB. From these observations, it can be concluded that SB responds better than AC to the increments of operation time and temperature toward FA and H_2 generation. Furthermore, as discussed in our last work [39], with the same particle size, reducing metals exhibit different values of standard reduction potential and electronegativity, where metals with low electronegativity and more negative reduction potential are more active toward water splitting. This is why Al is better than Zn for activating H_2 generation, thanks to its more negative value of standard reduction potential of −1.676, against −0.7618 for Zn.

3.2. *Performance of selected metals and catalysts for the reduction of capture CO_2*

Table 1 shows that measured particle size of Al and Zn fine powders are almost equal (18.9 ± 0.6 μm and 19.6 ± 2.1 μm, respectively), thus allowing discarding its possible influence on the hydrogen generation results, being known that hydrogen release is highly dependable of this parameter [36]. Fig. 2 plots the yield, conversion and selectivity of FA and final H_2 partial pressure in the reactor as a function of the catalyst and reducing metal type, at 120 °C and 2 h. Catalyst Pd5AC showed the highest activity toward FA formation, up to 21.6 ± 3.2 %, with a calculated TON = 195, when using Al as reductant, and a negligible yield of 0.33 ± 0.05 % with Zn (TON = 2.98), associated to a lower final H_2 partial pressure. Also, as aforementioned, Zn has a less negative standard reduction potential, hence a lower availability of H_2, affecting the FA yield even with active catalyst Pd5AC. The resulting yield of the system Al/Pd5AC is comparable to our previous publication (i.e. 21.1 ± 1.9 %) [15], under the same conditions of 120 °C, 2 h, Al:AC molar ratio of 6 and 70 % volume filling. Catalyst Ru5AC showed a marginal FA yield, only when using Al as reductant, of 1,95 % (TON = 18.8), associated to a lower surface area (844.39 m^2/g), lower metallic dispersion and larger particle size, as will be discuss later. This allowed concluding that Pd5AC catalyst presents an overall better performance than Ru5AC, in accordance to E. González et al. [17]. For its part, Pt5AC catalyst showed inactivity toward FA formation with both metals, and this could be attributed to its higher activity toward the decomposition of formate into H_2 and CO_2 [37]. Comparing with literature results, Su et al conducted similar experiments with carbamate in ethanol, but under high pressure (2.75 MPa) of hydrogen during 1 h reaction in anhydrous ethanol at 20 °C, where Ru and Pt 5 % over AC were nearly inactive, and Pd5AC was the catalyst with the best performance [38]. Likewise, for a

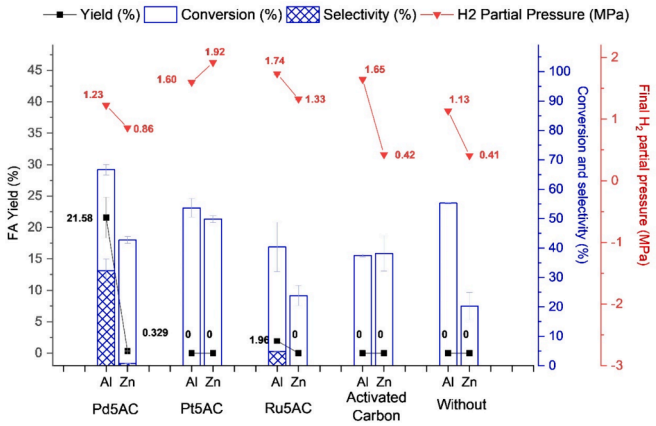

Fig. 2. Catalytic performance of different metal/catalyst systems in terms of FA yield and selectivity, AC conversion and final H_2 partial pressure. Reaction conditions: 2 h, metal:carbamate molar ratio of 6, catalyst metal:carbamate molar ratio of 3.8 mmol, 70 % of filling and 0.5 M of initial concentration.

Table 1
Textural properties of solids before reaction.

Sample	Surface area (m^2/g)	Pore volume (cm^3/g)	Pore size (Å)	Particle size – d90 (μm)
Pd5AC	948.96	0.44	55.05	–
Pt5AC	1490.63	0.81	58.74	–
Ru5AC	844.39	0.36	57.05	–
Al fine-powder	0.04	0	29.49**	18.87 ± 0.6*
Zn fine-powder	0.24	0	77.1***	19.61 ± 2.1*

* d90 percentile (Mastersizer).
** by DFT (Density Functional Theory).
*** by BET.

similar TON = 162 (FA yield of 17.6 %) Su *et al* used high pressure of hydrogen (2.75 MPa) and ethanol 30 %. The benefits were the decrease in temperature (20 °C) and time (1 h). This means that intake of ethanol, which adds an extra cost, can be compensated by a cheaper reductant like aluminum, preferably from residues for economic feasibility, and mild temperature reaction, with the possibility of *in-situ* generating green hydrogen.

3.3. Effect of type of catalyst in the H_2 yield

For most of the catalysts, Al produced higher H_2 final partial pressure than Zn, up to 1.74 MPa (with Ru5AC). The difference is more appreciable in control experiments with activated carbon and without catalyst (up to 1.65 MPa with Al and 0.42 MPa with Zn) (see Fig. 2). Likewise, Fig. 3 presents the comparison of FA and hydrogen yield for all metal/catalyst combinations, where, accordingly to the pressure, Al produced a higher H_2 yield (10.6 %) than Zn (8.64 %), with the most active catalyst Pd5AC. The H_2 yield (4.4 %) from experiments without catalyst, being non-zero, suggests that carbonaceous supports may play a role in the H_2 generation, where the reducing metal powder is dispersed onto the support's high surface area, thus increasing the contact area between metal and water. In this sense, the higher surface area of Pt5AC (1490.6 m^2/g) and Zn powder (0.24 m^2/g), may have contributed to the highest yield with Zn of 19.7 %, along with the fact that this catalyst is active toward decomposition of formate into H_2 and CO_2, as discussed before. Besides, as will be discussed later on the light of TPR analysis, the higher H_2 yield observed for Pt and Ru catalysts might be associated with the fact that these catalysts, at the reaction conditions studied, unlikely tend to adsorb H_2 to form hydrides, in contrast to Pd catalyst which tends to adsorb H_2 by forming both superficial and strong Pd-Hydrides, supporting the influence of the nature of the noble metal on the hydrogen evolution and the subsequent capture CO_2 reduction step (see Fig. 2S).

3.4. XRD results

The solid residues after reaction with Al and Zn, using Pd5AC as catalyst, were characterized by XRD to determine oxidized by-products. Fig. 4 shows the analyses of remaining unreacted elementary metals (Al and Zn) along with a mixture of oxides and hydroxides. Carbonates were also detected, suggesting that part of the conversion of carbamate is due to the formation of these compounds. From this, can be concluded that, under the reaction conditions studied, i) a complete conversion of the elementary metals is difficult to achieve in 2 h, and ii) reducing metals can react with the CO2RS, taking place an intake or re-capture of CO_2 to form carbonates.

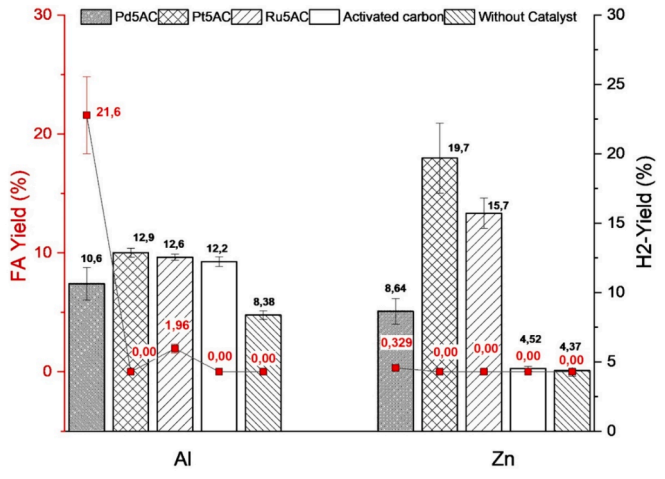

Fig. 3. FA and H_2 yield for the different metal/catalyst systems. Reaction conditions: 2 h, metal:carbamate molar ratio of 6, catalyst metal:carbamate molar ratio of 3.8 mmol, 70 % of filling and 0.5 M of initial concentration.

3.5. SEM observations

The solid samples after reaction with Al and Zn, in presence of Pd5AC, were surface characterized by SEM-BSE. In this technique, the intensity of the backscattered-electrons (BSE) correlates with larger atoms (greater weight and atomic number Z), appearing as brighter areas, while dark areas are smaller atoms with lower number [40]. In Fig. 5 a), a smooth bright layer of aluminum hydroxides and carbonates (detected by XRD) appear covering the surface of round shapes of unreacted elementary aluminum. Fig. 5 b) reflects the oxidation of pure zinc to form ZnO (lighter areas), by the appearance of crystalline microstructures with needle like shapes. The globular darker shapes can be ascribed to the carbon support, and unreacted metal.

3.6. H_2-TPR analyses

The temperature programed reduction technique is a useful tool for determining the different oxidation state species of a catalyst. These analyses were conducted to understand the behavior of the metal-active sites of the catalysts before and after the process of reduction of carbamate, using pure-hydrogen as reducing agent to avoid possible interactions of reducing metals (Al and Zn) with the technique.

From H_2 consumption curves before reaction for Pd5AC (Fig. 6) a positive peak is present with a maximum at temperature 225 °C, which corresponds to PdO species strongly interacting with the support [41], where a complete reduction of Pd (II) to Pd (0) takes place [42]. This event is followed by a wider peak with maximum H_2 consumption at 607 °C, ascribable to gasification of the carbon lattice, that usually onsets from 600 °C for carbon supports [43,44]. After reaction, Pd5AC catalyst presented only a negative peak beginning at 293.7 °C, which has been reported as the critical point (Tc) of the palladium hydride system (PdH_x, x = 0.205) [45], reaching a maximum peak at 315 °C. This behavior means that, during the TPR, hydrogen was desorbed/released from the catalyst, instead of consumed, and was also found in the reduction of capture CO_2 to formate in our previous report [15]. This phenomenon is related to the decomposition of a metal-hydride, suggesting the possible existence of palladium hydride PdH, which is a reducing specie. For a reaction temperature of 120 °C, and a Tc of PdH system of 293.7 °C, the activity of a possible hydride should remain during the whole process. Nevertheless, further characterization should be undergone to fully characterize Pd-hydride species in the catalyst after reaction. Also, no peaks of oxides reduction were evident after reaction, meaning a low deactivation by oxidation. Therefore, the superiority of Pd5AC catalyst can be summarized in three main facts: i) possible active palladium hydride specie was formed during the mild reaction temperature given its negative enthalpy of formation, a conditions required to favor its formation at low temperature and pressure [46,47], ii) the palladium low heat of hydrogen absorption, compared to other metals like Ni and Pt [48,49], and iii) palladium promotes the diffusion of h protons throughout the carbon support by a hydrogen spillover mechanism [50].

The null activity of Pt5AC catalyst observed in the catalytic experiments is consistent with the TPR profiles before and after reaction, where no significant consumption of hydrogen was observed, meaning that most of the Pt is in reduced state, but remained unchanged during the carbamate to formate process. The deficient performance of Pt5AC can be explained by an insufficient hydrogen pressure (2.5 MPa) to form active hydride species, which in this case requires much higher pressures of at least 27 GPa [51].

TPR curve for Ru5AC, before reaction, shows a flat behavior, indicating that the catalyst is completely reduced. However, after reaction the catalyst presented a greater oxygen elimination of 0.3 g/g_{cat} (compared to Pd5AC and Pt5AC) with a single significant peak appearing at 321 °C, ascribable to oxidation state Ru (III) [52,53],

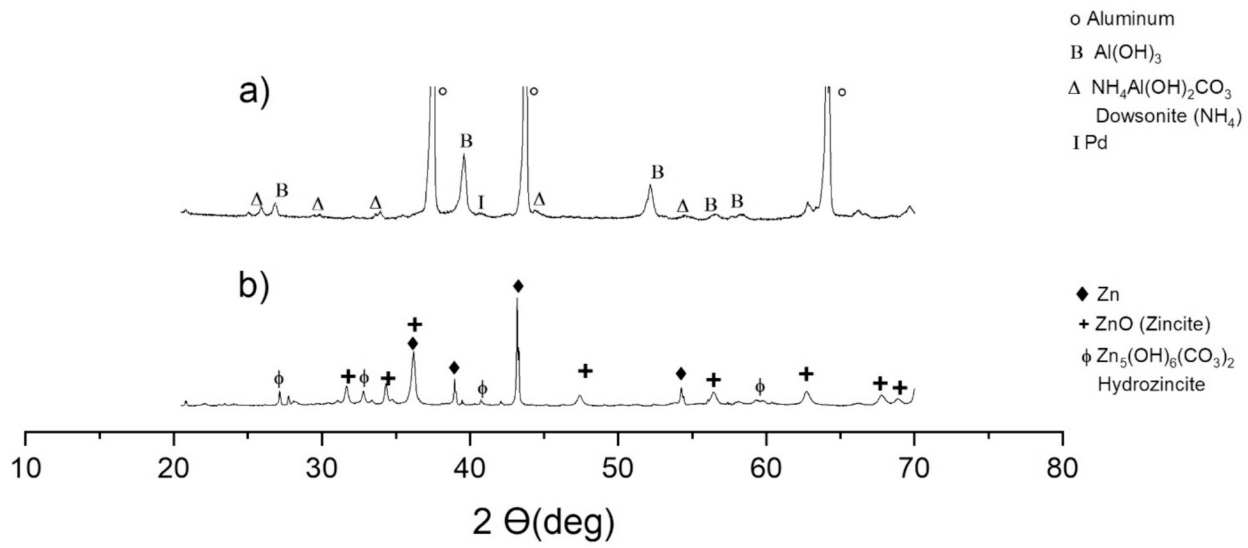

Fig. 4. XRD diffractograms of solid residue after reaction with catalyst Pd5AC and metals a) Al, and b) Zn. Reaction conditions: 120 °C, 2 h, metal:carbamate molar ratio of 6, catalyst metal:carbamate molar ratio of 3.8 mmol, 70 % of filling and 0.5 M of initial concentration.

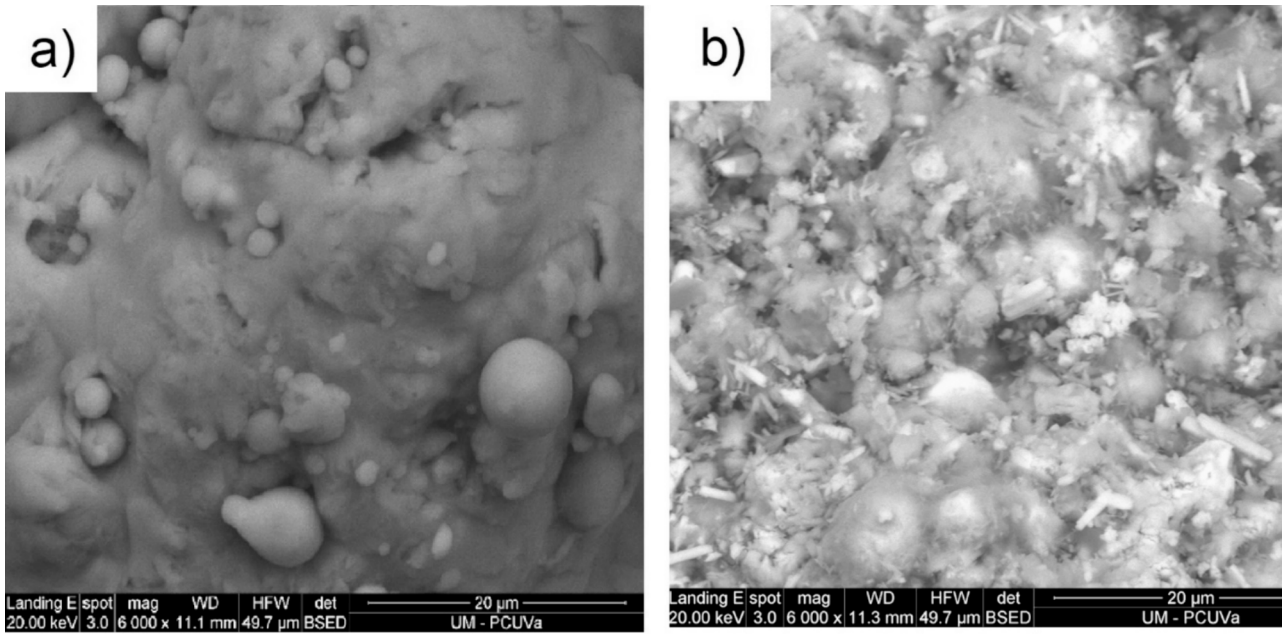

Fig. 5. Micrographs of solid residues after reduction with powder of a) Al and b) Zn. Reaction conditions: 120 °C, 2 h, metal:carbamate molar ratio of 6, catalyst metal:carbamate molar ratio of 3.8 mmol, 70 % of filling and 0.5 M of initial concentration.

revealing that this catalyst quickly deactivated during the process and did not develop metallic hydrides, reflected in the low formate yield of 1.76 % (see Table 2). Although ruthenium, similarly as platinum, cannot form stable hydrides at moderate pressures [54], the observed activity of Ru5AC catalyst can be understood by the ability of reduced ruthenium to adsorb and desorb hydrogen over its metallic surface, generating empty coordination sites that allows co-adsorption of reactant molecules and its conversion by hydrogen transfer [55].

3.7. TEM images analyses

Fig. 3S depicts selected images of all catalysts tested, clearly observing that most of the nanoparticles are round and dispersed, with gauss (Pd5AC) and Lognormal (Pt and Ru5AC) distributions. The particle size measured for Pd5AC (3.81 nm) is consistent with previous reports of similar catalysts comprising 5 % palladium over carbon, ranging between 3–5 nm (based on TEM and CO chemisorption analyses) and metallic dispersion of 17–25 % [17,56,57,38]. For its part, platinum and ruthenium catalysts presented comparatively poor dispersions of about 15 % (Table 2), with larger particle sizes ranging between 6.6–7.11 nm, features known to strongly affect the catalytic activity [58], as observed before when comparing the selected catalyst for the reduction of carbamate.

4. Conclusions

Among the tested catalysts, Pd5AC displayed the best performance toward formate yield from CO_2 captured in aqueous ammonia, because of its high dispersion (29.4 %) and low deactivation by oxidation and was the only catalyst to show insights of formation of possible active

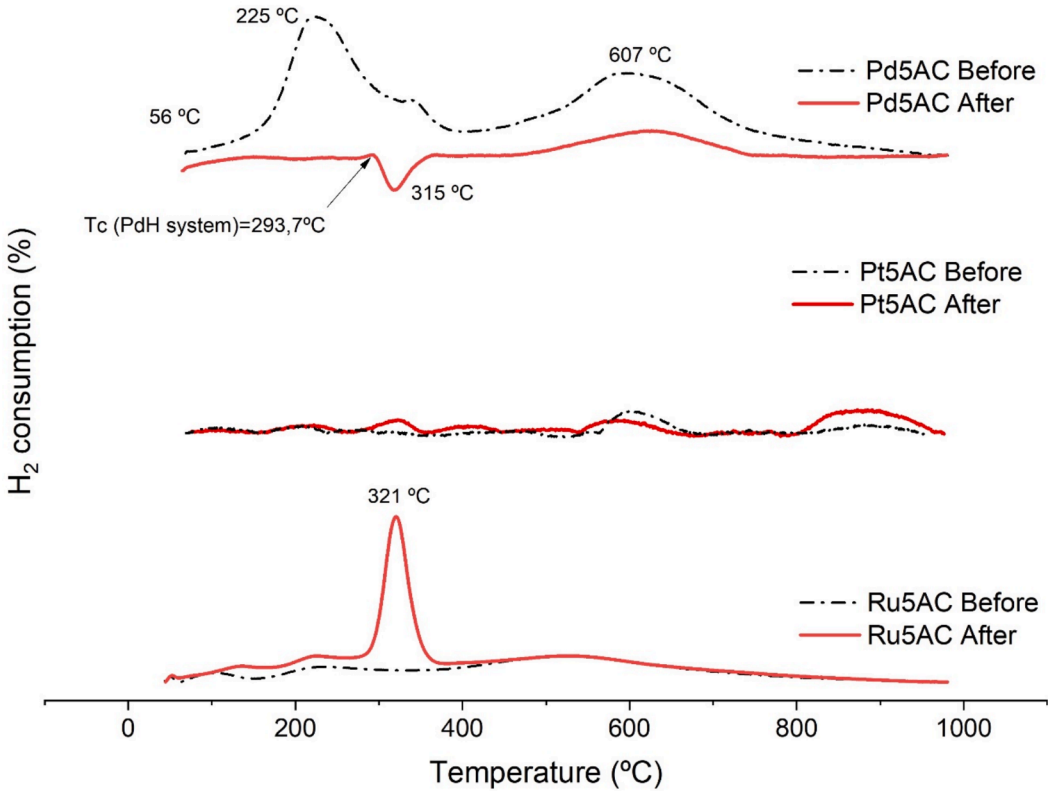

Fig. 6. H_2-TPR curves of catalysts Pd5AC, Pt5AC and Ru5AC before and after reduction of carbamate with pure-hydrogen. Reaction conditions: 2 h, 2.5 MPa of 99.99 % pure-hydrogen, catalyst metal:carbamate molar ratio of 3.8 mmol, 70 % of filling and 0.5 M of initial concentration.

Table 2
Formate yield and oxygen elimination during H_2-TPR characterization of catalysts. Reaction conditions: 2 h, 2.5 MPa of 99.99 % pure-hydrogen, 70 % of filling and 0.5 M of AC initial concentration.

Sample	Particle size (nm)*	Dispersion (%)*	FA yield (%)	TON	Oxygen eliminated (g/g)	
					Before reaction	After reaction
Pd5AC	3.81 ± 1.98	29.44 %	38.98 ± 2.3	357.7	0.18	0.12
Pt5AC	7.11 ± 5.0	15.18 %	0	0	0.15	0.14
Ru5AC	6.59 ± 5.2	15.77 %	1.76 ± 0.01	16.6	0.17	0.30

* By TEM image analysis.

hydride species. Although Zn displayed a certain formate yield (0.33 %), aluminum was the most efficient, up to 21.6 %, while presenting faster H_2 generation rates than Zn. Both CO2RS/CO2LS streams showed activation of the hydrogen generation, and this effect was strongly influenced by initial pH. The present study suggests that both type of streams are potential hydrothermal media for hydrogen generation and formic acid production, which are value-added chemicals with increasing markets in the short term. This represents a potential integration of carbon capture utilization and storage (CCUS) with the hydrogen production in the frame CO_2 and H_2 economies.

CRediT authorship contribution statement

Juan I. del Río: Writing – original draft, Investigation. **Miguel Almarza:** Investigation. **Ángel Martín:** Writing – review & editing, Supervision, Funding acquisition, Conceptualization. **María D. Bermejo:** Writing – review & editing, Supervision, Project administration, Methodology, Funding acquisition, Conceptualization.

Declaration of competing interest

The authors declare the following financial interests/personal relationships which may be considered as potential competing interests: Angel Martin reports financial support was provided by Junta de Castilla y León Consejería de Educación. Angel Martin reports financial support was provided by Fundación Naturgy. Juan Ignacio del Rio reports financial support was provided by Colombia Ministry of Science Technology and Innovation. If there are other authors, they declare that they have no known competing financial interests or personal relationships that could have appeared to influence the work reported in this paper.

Data availability

No data was used for the research described in the article.

Acknowledgements

This project has been funded by Junta de Castilla y León through FEDER FUNDS under the BioEcoUVa Strategic Program (CLU-2019-04), and by Fundación Naturgy through the 1st Award to Research and Innovation in the Energy Sector. Juan Ignacio del Río gratefully acknowledges Universidad de Valladolid for the predoctoral and postdoctoral fellowships, and the financial support provided by the Ministry of Science, Technology and Innovation of Colombia within the framework of the call No. 914-2022 (Contract No. 80740-098-2022).

Appendix A. Supplementary data

Supplementary data to this article can be found online at https://doi.org/10.1016/j.fuel.2024.132146.

References

[1] Bashir MF. Oil price shocks, stock market returns, and volatility spillovers: a bibliometric analysis and its implications. Environ Sci Pollut Res 2022;29:22809–28.

[2] Nocito F, Dibenedetto A. Atmospheric CO_2 mitigation technologies: carbon capture utilization and storage. Curr Opin Green Sustainable Chem 2020;21:34–43. https://doi.org/10.1016/j.cogsc.2019.10.002.

[3] Hekmatmehr H, Esmaeili A, Pourmahdi M, Atashrouz S, Abedi A, Ali Abuswer M, et al. Carbon capture technologies: a review on technology readiness leve. Fuel 2024;363:130898. https://doi.org/10.1016/j.fuel.2024.130898.

[4] Al Baroudi H, Awoyomi A, Patchigolla K, Jonnalagadda K, Anthony EJ. A review of large-scale CO_2 shipping and marine emissions management for carbon capture, utilisation and storage. Appl Energy 2021;287:116501. https://doi.org/10.1016/j.apenergy.2021.116510.

[5] Valluri S, Claremboux V, Kawatra S. Opportunities and challenges in CO_2 utilization. J Environ Sci 2022;113:322–44.

[6] Koytsoumpa EI, Bergins C, Kakaras E. The CO_2 economy: review of CO_2 capture and reuse technologies. J Supercrit Fluids 2017;132:3–16. https://doi.org/10.1016/j.supflu.2017.07.029.

[7] Chen X, Gao R, Qiang W, Kehao H, Wang F, Deng C, et al. Direct hydrogenation of CO_2 to liquid hydrocarbons over K/Fe-C catalysts: effect of porous carbon matrix and K modification. Fuel 2024;364:131031. https://doi.org/10.1016/j.fuel.2024.131061.

[8] Andérez-Fernández M, Ferrero S, Queiroz JPS, Pérez E, Álvarez CM, Martín A, et al. Formic acid production by simultaneous hydrothermal CO_2 reduction and conversion of glucose and its derivatives. J Taiwan Inst Chem Eng 2022;139:104504. https://doi.org/10.1016/j.jtice.2022.104504.

[9] Jarvis SM, Samsatli S. Technologies and infrastructures underpinning future CO_2 value chains: a comprehensive review and comparative analysis. Renew Sustain Energy Rev 2018;85:46–68.

[10] Jin F, Gao Y, Jin Y, Zhang Y, Cao J, Wei Z, et al. High-yield reduction of carbon dioxide into formic acid by zero-valent metal/metal oxide redox cycles. Energy Environ Sci 2011;4(3):881–4. https://doi.org/10.1039/C0EE00661K.

[11] Najafabadi AT. CO_2 chemical conversion to useful products: an engineering insight to the latest advances toward sustainability. Int J Energy Res 2013;37(6):485–99.

[12] Wang W, Xiang M, Fy Y, Wang W, Duan J. Three-dimensional porous Cu-Zn/NF catalysts for efficient photocatalytic reduction of CO_2 in alkaline environment for methanol preparation in a monolithic microreactor. Fuel 2024;357:129778. https://doi.org/10.1016/j.fuel.2023.129778.

[13] Liu X, Zhong H, Wang C, He D, Jin F. CO_2 reduction into formic acid under hydrothermal conditions: a mini review. Energy Sci Eng 2022;10(5):1601–13.

[14] Verma P, Zhang S, Song S, Mori K, Kuwahara Y, Wen M, et al. Recent strategies for enhancing the catalytic activity of CO_2 hydrogenation to formate/formic acid over Pd-based catalyst. J CO_2 Util 2021;54:101765. https://doi.org/10.1016/j.jcou.2021.101765.

[15] Del Río JI, Pérez E, León D, Martín A, Bermejo MD. Catalytic hydrothermal conversion of CO_2 captured by ammonia into formate using aluminum-sourced hydrogen at mild reaction conditions. J Ind Eng Chem 2021;97:539–48.

[16] Hao C, Wang S, Li M, Kang L, Ma X. Hydrogenation of CO_2 to formic acid on supported ruthenium catalysts. Catal Today 2011;160(1):184–90. https://doi.org/10.1016/j.cattod.2010.05.034.

[17] González E, Marchant C, Sepúlveda C, García R, Ghampson IT, Escalona N, et al. Hydrogenation of sodium hydrogen carbonate in aqueous phase using metal/activated carbon catalysts. Appl Catal B Environ 2018;224:368–75.

[18] Huang Z. CO_2 hydrogenation over mesoporous Ni-Pt/SiO_2 nanorod catalysts: determining CH_4/CO selectivity by surface ratio of Ni/Pt. Chem Eng Sci 2022;247:117106.

[19] Ma Z, Li P, Ye L, Wang L, Xie H, Zhou Y. Selectivity reversal of photocatalytic CO_2 reduction by Pt loading. Catal Sci Technol 2018;8(20):5129–32.

[20] Zhang QH, Han WD, Hong YJ, Yu JG. Photocatalytic reduction of CO_2 with H_2O on Pt-loaded TiO_2 catalyst. Catal Today 2009;148(3–4):335–40.

[21] Umeda M, Niitsuma Y, Horikawa T, Matsuda S, Osawa M. Electrochemical reduction of CO_2 to methane on platinum catalysts without overpotentials: strategies for improving conversion efficiency. ACS Appl Energy Mater 2019;3(1):1119–27.

[22] Valekar AH, Oh KR, Lee SK, Hwang YK. Simultaneous production of lactate and formate from glycerol and carbonates over supported Pt catalysts. J Ind Eng Chem 2021;101:66–77.

[23] Gunasekar GH, Park K, Jung KD, Yoon S. Recent developments in the catalytic hydrogenation of CO_2 to formic acid/formate using heterogeneous catalysts. Inorg Chem Front 2016;3(7):882–95.

[24] Yan N, Philippot K. Transformation of CO_2 by using nanoscale metal catalysts: cases studies on the formation of formic acid and dimethylether. Curr Opin Chem Eng 2018;20:86–92. https://doi.org/10.1016/j.coche.2018.03.006.

[25] Singh AK, Singh S, Kumar A. Hydrogen energy future with formic acid: a renewable chemical hydrogen storage system. Catal Sci Technol 2016;6(1):12–40. https://doi.org/10.1039/c5cy01276g.

[26] Gürsel IV, Noël T, Wang Q, Hessel V. Separation/recycling methods for homogeneous transition metal catalysts in continuous flow. Green Chem 2015;17(4):2012–26.

[27] Jin F, Zeng X, Liu J, Jin Y, Wang L, Zhong H, et al. Highly efficient and autocatalytic H_2O dissociation for CO_2 reduction into formic acid with zinc. Sci Rep 2014;4:4503. https://doi.org/10.1038/srep04503.

[28] Krokidis X, Raybaud P, Gobichon AE, Rebours B, Euzen P, Toulhoat H. Theoretical study of the dehydration process of boehmite to γ-alumina. J Phys Chem B 2001;105(22):5121–30.

[29] Lopes OF, Mendonca VR, Umar A, Chuahan MS, Kumar R, Chauhan S, et al. Zinc hydroxide/oxide and zinc hydroxy stannate photocatalysts as potential scaffolds for environmental remediation. New J Chem 2015;39(6):4624–30. https://doi.org/10.1039/c5nj00324e.

[30] Bacelo H, Pintor AMA, Santos SCR, Boaventura RAR, Botelho CMS. Performance and prospects of different adsorbents for phosphorus uptake and recovery from water. Chem Eng J 2019;381:122566. https://doi.org/10.1016/j.cej.2019.122566.

[31] Charvin P, Abanades S, Lemort F, Flamant G. Hydrogen production by three-step solar thermochemical cycles using hydroxides and metal oxide systems. Energy Fuel 2007;21(5):2919–28.

[32] Ishaq H, Dincer I, Crawford C. A review on hydrogen production and utilization: challenges and opportunities. Int J Hydrogen Energy 2022;47(62):26238–64.

[33] Zhong H, Wang L, Yang Y, He R, Jing Z, Jin F. Ni and Zn/ZnO synergistically catalyzed reduction of bicarbonate into formate with water splitting. ACS Appl Mater Interfaces 2019;11(45):42149–55.

[34] Umpierre AP, de Jesus E, Dupont J. Turnover numbers and soluble metal nanoparticles. ChemCatChem 2011;3(9):1413–8.

[35] Sevjidsuren G. Effect of different support morphologies and Pt particle sizes in electrocatalysts for fuel cell applications. J. Nanomater 2010:852786.

[36] Razavi-Tousi SS, Szpunar JA. Effect of structural evolution of aluminum powder during ball milling on hydrogen generation in aluminum–water reaction. Int J Hydrogen Energy 2013;38(2):795–806.

[37] Fujitsuka H, Nakagawa K, Hanprerakriengkrai S, Nakagawa H, Tago T. Hydrogen production from formic acid using Pd/C, Pt/C, and Ni/C catalysts prepared from ion-exchange resins. J Chem Eng Japan 2019;52(5):423–9.

[38] Su J, Lu M, Lin H. High yield production of formate by hydrogenating CO_2 derived ammonium carbamate/carbonate at room temperature. Green Chem 2015;17(5):2769–73.

[39] Del Rio JI, Martin A, Bermejo MD. Coupling the solvent-based CO_2 capture processes to the metal water-splitting for hydrogen generation in a semi-continuous system. Int J Hydrogen Energy 2023;48(72):27892–906.

[40] Wang ZL, Liu Y, Zhang Z. Handbook of nanophase and nanostructured materials. Mater Syst Appl I 2003;3.

[41] Aznarez A, Gil A, Korili SA. Performance of palladium and platinum supported on alumina pillared clays in the catalytic combustion of propene. RSC Adv 2015;5(100):82296–309.

[42] Juszczyk W. Characterization of supported palladium catalysts: III. $PdAl_2O_3$. J Catal 1989;120(1):68–77. https://doi.org/10.1016/0021-9517(89)90251-0.

[43] Trépanier M, Tavasoli A, Dalai AK, Abatzoglou N. Co, Ru and K loadings effects on the activity and selectivity of carbon nanotubes supported cobalt catalyst in Fischer-Tropsch synthesis. Appl Catal A Gen 2009;353(2):193–202.

[44] Zhang G, Li Z, Zheng H, Fu T, Ju Y, Wang Y. Influence of the surface oxygenated groups of activated carbon on preparation of a nano Cu/AC catalyst and heterogeneous catalysis in the oxidative carbonylation of methanol. Appl Catal B Environ 2015;179:95–105.

[45] Manchester FD, San-Martin A, Pitre JM. The H-Pd (hydrogen-palladium) system. J Phase Equilibria 1994;15(1):62–83.

[46] Kohlmann H. Metal hydrides, in Encyclopedia of Physical Science and Technology. 3rd ed. Elsevier; 2003.

[47] Yang X, Li H, Ahuja R, Kang T, Luo W. Formation and electronic properties of palladium hydrides and palladium-rhodium dihydride alloys under pressure. Sci Rep 2017;7(1):3520.

[48] Christensen OB, Stoltze P, Jacobsen KW, Nrskov JK. Effective-medium calculations for hydrogen in Ni, Pd, and Pt. Phys Rev B 1990;41(18):12413.

[49] Andreasen A. Predicting formation enthalpies of metal hydrides. Roskilde, Denmark: Risø-Risø National Laboratory; 2004.

[50] Adams BD, Chen A. The role of palladium in a hydrogen economy. Mater Today 2011;14(6):282–9. https://doi.org/10.1016/S1369-7021(11)70143-2.

[51] Scheler T. Synthesis and properties of platinum hydride. Phys Rev B 2011;83(21).

[52] Man B. Oxidation modification of Ru-based catalyst for acetylene hydrochlorination. RSC Adv 2017;7(38):23742–50.

[53] Zhang Z. Ru-Co (III)-Cu (II)/SAC catalyst for acetylene hydrochlorination. Appl Catal B Environ 2016;189:56–64.

[54] Kuzovnikov MA, Tkacz M. Synthesis of ruthenium hydride. Phys Rev B 2016;93(6):64103.

[55] Müller TE. Hydrogenation and Hydrogenolysis with Ruthenium Catalysts and Application to Biomass Conversion. In: Ruthenium An Element Loved by Researchers, Ed. Intechopen; 2021.

[56] Neri G, Musolino MG, Milone C, Pietropaolo D, Galvagno S. Particle size effect in the catalytic hydrogenation of 2, 4-dinitrotoluene over Pd/C catalysts. Appl Catal A Gen 2001;208(1–2):307–16.

[57] Rozmysłowicz B, Maki-Arvela P, Tokarev A, Leino AR, Eranen K, Murzin DY. Influence of hydrogen in catalytic deoxygenation of fatty acids and their derivatives over Pd/C. Ind Eng Chem Res 2012;51(26):8922–7.

[58] Jeong H, Kwon O, Kim BS, Bae J, Shin S, Kim HE, et al. Highly durable metal ensemble catalysts with full dispersion for automotive applications beyond single-atom catalysts. Nat Catal 2020;3(4):368–75.